INTERNATIONAL JOURNAL FOR NUMERICAL METHODS IN FLUIDS, VOL. 13, 869–882 (1991)

A MOVING GRID METHOD APPLIED TO ONE-DIMENSIONAL NON-STATIONARY FLAME PROPAGATION

A. MACK, H. J. WEBER AND P. ROTH*

Fachgebiet Verbrennung und Gasdynamik, Universität Duisburg, W-4100 Duisburg, F.R.G.

SUMMARY

The paper presents applications of a moving grid method to the combined problem of ignition and premixed flame propagation in a closed vessel. This method belongs to the general class of adaptive grid techniques for the numerical integration of evolutionary partial differential equations and is based on the method of lines with variable node position. In the present case the motion of the grid and the solution of the partial differential equations are strongly coupled by an implicit formulation. The problem is reduced to an initial value problem for a stiff differential–algebraic system. The continuously moving grid is determined by the equidistribution of a positive function which depends on the solution of the partial differential equations. A differential–algebraic system solver is used for the time integration of the initial value problem. The numerical results of the test problems demonstrate the computational efficiency and the capability of the method to resolve the main features of the solution.

KEY WORDS Flame propagation Moving grid method Combustion Method of lines Differential algebraic system

1. INTRODUCTION

Premixed, laminar flame propagation is a basic topic in combustion modelling. The mechanism that drives a premixed flame is a self-sustaining interaction between convection, diffusion and chemical reactions within the flame zone.[1] The corresponding mathematical model consists of a highly non-linear parabolic initial value problem. This system exhibits a temporal stiffness owing to the presence of exponential reaction rate source terms and a spatial stiffness because of the large ratio of combustion chamber length to flame thickness. The moving flame front is characterized by a region with steep spatial gradients and its velocity depends strongly on the processes in the thin flame zone. This is in contrast to purely hydrodynamical fluid flow, e.g. shock wave propagation, where the speed of the shock is only influenced by the flow conditions outside the shock. These aspects require the application of a non-uniform time-dependent grid with a high resolution in the entire flame front and an implicit time discretization.[2]

In recent years, two major approaches using the method of lines have been developed to treat these problems. In the first approach the temporal derivatives in the governing equations were discretized by finite differences and the resulting boundary value problem was solved.[2] This method offers the advantage of incorporating the knowledge that has been collected from solving elliptic boundary value problems. The results described in the literature concerning non-uniform

* Author to whom correspondence should be addressed.

0271–2091/91/170869–14$07.00

Received July 1990
Revised December 1990

grids in conjunction with the numerical treatment of two-point boundary value problems[3,4] can be carried over into the development of numerical methods for one-dimensional stiff partial differential equations (PDEs).

This paper follows the second approach, in which the spatial derivatives of the PDE system are discretized by finite elements of finite differences. This development is motivated by the availability of sophisticated solvers for differential–algebraic equations, e.g. the extrapolation code LIMEX[5] and the backward difference code DASSL.[6] This semidiscretization converts the initial boundary value problem into an initial value problem for a differential–algebraic equation (DAE) system with a continuous time derivative. The moving finite element (MFE) method belongs to this class of methods. It uses a variational formulation of the governing equations, generates an ordinary differential equation (ODE) system for the grid points and formulates the physical variables in these moving nodes.[7] Applications and further investigations of the MFE method can be found in References 8–10. A major concept in the MFE method is a penalty function, which regularizes the grid movement. This additional tuning of the grid selection seems to be a diminishing factor for reliability.[11] The method described in Reference 12 uses the DAE formulation with a spatial finite difference discretization, a variable number of nodes and a static regridding strategy, which can change the order of the DAE system and requires the interpolation of the solution values from the old onto the new grid. This procedure interrupts the time-stepping process and does not allow higher-order schemes for the temporal discretization in the DAE solver. The same problem is discussed in the investigation of method I in Reference 11.

The numerical method applied in the present paper is based on a moving grid method discussed in Reference 11. The grid selection strategy was described in Reference 13 in connection with a shock tube and an astrophysical simulation problem. This method consists of a semidiscretization of the governing equation with a fixed number of nodes in a moving co-ordinate system, which results in a DAE system for each node. The system is completed by a set of quasi-linear implicit ordinary differential equations for the motion of each grid point, which depends on the numerical approximation of the solution in the nodes. The grid points are distributed in such a way that a given positive function, e.g. the arc length of the solution, is equidistributed over the entire region. It must be pointed out that at each time step the new grid is calculated simultaneously with the approximated solution of the partial differential equations. This fully implicit formulation avoids regridding and interpolation procedures. As a consequence, the backward difference DAE solver DASSL can operate with higher-order discretization schemes and larger time steps. The computational efficiency is demonstrated by two test problems, in which the propagation of a confined flame with full chemistry including ignition and extinction was numerically simulated. The method shows the capability to detect regions where ignition occurs and the flame front is created. Later on the grid moves with the highly resolved propagating combustion front until the flame reaches the wall of the vessel or a homogenous ignition of the unburnt gas occurs.

2. GOVERNING EQUATIONS

The equations which describe the behaviour of a reacting gas flow include non-linear phenomena as, for example, in shock waves and reaction–diffusion equations.[14] In the present case the formation and propagation of a combustion wave in a slowly reacting environment was studied. The deflagration occurs in a heat-conducting gas owing to the initiation of exothermic chemical reactions. The conduction of the heat released and the diffusion of highly reactive components then lead to the formation of a flame front, which propagates into the unburnt gas mixture. Gas dynamic effects are of minor importance in this low-Mach-number regime. This condition justifies the assumption of a spatially uniform pressure. The resulting mathematical model for

one-dimensional confined flame propagation was derived from the conservation equations of species mass, energy, linear momentum and total mass and the equation of state in Lagrangian mass co-ordinates. The transformation into the Lagrangian co-ordinate system eliminates the convective terms in the partial differential equations and simplifies the numerical treatment. The mathematical model considered here consists of the following mixed algebraic and partial differential equation system in Lagrangian co-ordinates:

$$\frac{\partial Y_i}{\partial t}+\frac{\partial(\rho Y_i V_i)}{\partial \psi}=\frac{\dot{r}_i}{\rho}, \quad i=1, \ldots, NST, \tag{1}$$

$$\frac{\partial T}{\partial t}-\frac{1}{\rho c_p}\frac{\partial p}{\partial t}+\frac{1}{c_p}\sum_{i=1}^{NST}\rho Y_i V_i c_{p_i}\frac{\partial T}{\partial \psi} -\frac{1}{c_p}\frac{\partial}{\partial \psi}\left(\lambda\rho\frac{\partial T}{\partial \psi}\right)+\frac{1}{\rho c_p}\sum_{i=1}^{NST}\dot{r}_i h_i=\frac{\dot{q}}{\rho c_p}, \tag{2}$$

$$\frac{\partial p}{\partial \psi}=0, \tag{3}$$

$$\frac{\partial z}{\partial \psi}=\frac{1}{\rho}, \tag{4}$$

$$p-R_M\rho T\sum_{i=1}^{NST}\frac{Y_i}{M_i}=0, \tag{5}$$

where $0<\psi<\psi_{max}$, $t>0$, ψ is the Lagrangian mass co-ordinate, t is time, z is the Eulerian co-ordinate, p is pressure, T is temperature, Y_i is the mass fraction of species i, ρ is the mass density, NST is the number of species, M_i is the mole fraction of species i, $\dot{r}_i$ is the molar rate of formation of species i, c_{p_i} is the specific heat capacity at constant pressure of species i, c_p is the specific heat capacity at constant pressure of the mixture, λ is the thermal conductivity of the mixture, V_i is the diffusion velocity of species i, h_i is the specific enthalpy of species i, R_M is the universal gas constant and $\dot{q}$ is the source term for external energy addition.

The initial and boundary conditions are

$$\begin{aligned}
&T(0,\psi)=T_0(\psi),\\
&Y_i(0,\psi)=Y_{i,0}(\psi), \quad i=1, \ldots, NST,\\
&p(0,\psi)=p_0,\\
&\frac{\partial T(t,0)}{\partial \psi}=0,\\
&\frac{\partial T(t,\psi_{max})}{\partial \psi}=0,\\
&\frac{\partial Y_i(t,0)}{\partial \psi}=0, \qquad i=1, \ldots, NST,\\
&\frac{\partial Y_i(t,\psi_{max})}{\partial \psi}=0, \qquad i=1, \ldots, NST,\\
&z(t,0)=0,\\
&z(t,\psi_{max})=z_{max}.
\end{aligned} \tag{6}$$

The vessel in which the combustible gas mixture is enclosed has an infinite slab geometry and a length z_{max} in Eulerian co-ordinates. The corresponding length ψ_{max} in Lagrangian mass co-ordinates can be calculated from

$$\psi(z, t) = \int_0^z \rho(x, t)\,\mathrm{d}x.$$

The quantity $\psi(z_{max}, t) = \psi_{max}$ is constant in time owing to the zero-mass-flux condition across the boundary for confined gas flow. The boundary conditions describe the fact that the walls are adiabatic and the mass flux through the walls is zero. Equations (1)–(5) have to be completed by formulae expressing the thermodynamic and transport properties λ, V_i, c_p, c_{p_i}, and h_i of the gas mixture. The reaction chemistry in front of the flame and in the flame zone must be expressed by the chemical source term $\dot{r}_i$ of the species i:

$$\dot{r}_i = M_i \sum_{j=1}^{k} \nu_{ij} R_j.$$

In this equation R_j is the reaction rate of the elementary reaction j and ν_{ij} is the stoichiometric coefficient of species i in the elementary reaction j. R_j has an exponential temperature dependence and a polynomial w_i-dependence. The source term $\dot{r}_i$ can be determined if the reaction mechanism is known.

In the present case the gas mixture was ignited owing to an artificial energy source term $\dot{q}$ which is defined by

$$\dot{q}(z, t) := \begin{cases} \dfrac{D}{t_i} \exp\left[-\left(\dfrac{z}{z_s}\right)^8\right], & 0 < t \leqslant t_i, \\ 0, & t > t_i, \end{cases}$$

where $0 < z < z_{max}$ and z_s denotes the thickness of the energy source, t_i the time interval for energy addition and D the density of source energy. The external energy source term has a smoothed-out rectangular shape.

3. DESCRIPTION OF THE MOVING GRID METHOD

A common feature of adaptive grid methods is to insert or to move grid points into regions with large spatial gradients in order to guarantee a high resolution of steep fronts and minimal truncation error of the spatial discretization. This situation is more complicated in the case of time-dependent problems where moving regions of high spatial activity are often encountered. A well-known approach is to formulate the original equations in a specific moving co-ordinate frame, e.g. in Lagrangian mass co-ordinates, in which the transformed problem is now stationary. This method is only suitable for problems with a constant propagation velocity or if the time-dependent co-ordinate transformation is known explicitly. In this section a moving grid method based on the investigations of Reference 11 is described in detail. In Reference 11 three different moving grid methods were tested with respect to reliability, robustness and efficiency.

The general class of evolutionary problems considered can be written in the abstract notation

$$\frac{\partial u}{\partial t}(x, t) = L[u(x, t)], \quad a < x < b, \quad t > 0, \tag{7}$$

where L represents a differential operator involving only spatial derivatives. The function $u(x, t)$ may exhibit the feature described above. The first step of the method consists of formulating the

partial differential equation in a moving co-ordinate system (ξ, τ). The main idea behind this time-dependent transformation is to smooth the temporal behaviour of u and to concentrate grid points in regions of high spatial activity. The co-ordinate transformation between x, t and the new variables ξ, τ is of the form

$$x = x(\xi, \tau), \qquad t = t(\xi, \tau) \equiv \tau. \tag{8}$$

Then the total time derivative $\mathrm{d}/\mathrm{d}t$ of u has been changed to

$$\frac{\mathrm{d}u}{\mathrm{d}t}(x(\xi, t), t) = \frac{\partial u}{\partial x}(x(\xi, t), t)\frac{\partial x}{\partial t}(\xi, t) + \frac{\partial u}{\partial t}(x(\xi, t), t). \tag{9}$$

With this time derivative the problem (7) can be transformed into the final evolutionary problem in the moving co-ordinate system

$$\frac{\mathrm{d}u}{\mathrm{d}t}(x(\xi, t), t) = \frac{\partial u}{\partial x}(x(\xi, t), t)\frac{\partial x}{\partial t}(\xi, t) + L[u(x(\xi, t), t)], \quad \xi(a) < \xi < \xi(b), \quad t > 0. \tag{10}$$

The specific transformation is strongly coupled to u through

$$\xi(x, t) = \frac{\int_a^x m(s, t)\mathrm{d}s}{\int_a^b m(s, t)\mathrm{d}s}, \quad a < x < b, \tag{11}$$

with the so-called monitor function $m(x, t)$ which may depend on u, u_x and u_{xx}:

$$m(x, t) = \Phi(u(x, t), u_x(x, t), u_{xx}(x, t)). \tag{12}$$

This function should reflect the spatial dependence of u and must be positive definite in order to guarantee the well-posedness of the transformation. The denominator in (11) normalizes the ξ-co-ordinate to the unit interval $0 < \xi < 1$. The main idea behind this formulation is to find a co-ordinate system which minimizes the modulus of the time derivative $(\mathrm{d}/\mathrm{d}t)(u(x(\xi, t), t))$. This would allow much larger time steps than in original formulation (7). This condition is violated during the formation of a front close to the right boundary. At that period of time $\partial u/\partial x$ and $\partial x/\partial t$ are positive. Therefore the total time derivative $\mathrm{d}u/\mathrm{d}t$ is greater than $\partial u/\partial t$ in (9). However, this behaviour changes when the front is resolved and starts to propagate.

In the next step an equidistribution principle is applied to (10) and (11). Consider an equidistant grid on [0, 1] for ξ with $NP+2$ grid points: $\xi_i = i/(NP+1)$, $i = 0, \ldots, NP+1$. With this uniform ξ-grid a non-uniform x-grid can be determined for a given u at time t through the transformation (11):

$$\int_{x_i}^{x_{i+1}} m(s, t)\mathrm{d}s = c(t), \quad i = 0, \ldots, NP, \tag{13}$$

with

$$c(t) = \frac{1}{NP+1}\int_a^b m(s, t)\mathrm{d}s. \tag{14}$$

Equation (13) shows the meaning of the equidistribution principle. The grid points are distributed in such a way that the integral of the monitor function m is equal to the quantity $c(t)$ on every interval (x_i, x_{i+1}), $i = 0, \ldots, NP$. The next relation gives the final condition for the non-uniform x-grid

$$a = x_0(t) < x_1(t) < \ldots < x_{NP}(t) < x_{NP+1}(t) = b \tag{15}$$

without calculating the specific quantity $c(t)$, i.e.

$$\int_{x_{i-1}}^{x_i} m(s,t)\mathrm{d}s = \int_{x_i}^{x_{i+1}} m(s,t)\mathrm{d}s, \quad i=1,\ldots,NP. \tag{16}$$

The positiveness of m implies a strictly increasing sequence $x_0,\ldots,x_{NP+1}$ which is preserved during the entire time integration procedure. This is an important feature because it prevents node crossing which creates severe numerical problems.

The spatial discretization of (10) leads to the semidiscrete formulation with the continuous variable t

$$\frac{\mathrm{d}U_i}{\mathrm{d}t}(t) = \frac{U_{i+1}(t)-U_{i-1}(t)}{X_{i+1}(t)-X_{i-1}(t)}\frac{\mathrm{d}X_i(t)}{\mathrm{d}t} + L_\Delta[\mathbf{U}(t)], \quad i=1,\ldots,NP, \tag{17}$$

where

$$X_i(t)=x(\xi_i,t), \qquad U_i(t)=u(x(\xi_i,t),t), \qquad \mathbf{U}(t)=(U_0(t),\ldots,U_{NP+1}(t))^{\mathrm{T}}$$

and L_Δ is the difference operator of L. Applying the midpoint rule to discretize (16) leads to the following algebraic system for the node positions:

$$(X_i-X_{i-1})M_{i-1}=(X_{i+1}-X_i)M_i, \quad i=1,\ldots,NP, \tag{18}$$

with

$$M_i(t)=m\left(\frac{X_{i+1}+X_i}{2},t\right).$$

The implicit ordinary differential equation system (17) together with the non-linear algebraic equations (18) represents a complete system for the time evolution of the grid points $X_i(t)$ and the approximate solution values $U_i(t)$ in these moving nodes. The values $U_0(t)$ and $U_{NP+1}(t)$ are determined by appropriate boundary conditions. The grid point trajectories $X_0(t)$ and $X_{NP+1}(t)$ are constant in time because of the fixed interval $[a,b]$ with $a=X_0(t)$ and $b=X_{NP+1}(t)$. The simultaneous solution of (17) and (18) offers no opportunity to smooth the grid motion in space and time and makes the entire differential–algebraic system extremely stiff. As a consequence, a DAE solver would take very small time steps for the time integration of the system.

A common approach to solve these problems is to determine the grid positions $X_i(t)$ by a set of differential equations derived from (18).[11,13] The first step consists of introducing the point concentrations n_i instead of the difference in the node positions:

$$n_i=\frac{1}{X_{i+1}-X_i}, \quad i=0,\ldots,NP. \tag{19}$$

With this definition, (18) is changed to

$$\frac{n_{i-1}}{M_{i-1}}=\frac{n_i}{M_i}, \quad i=1,\ldots,NP. \tag{20}$$

In order to prevent excessive grid distortion, the next step is to restrict the variations in the grid point concentration according to the following inequality:[13]

$$\frac{\kappa}{\kappa+1}\leqslant\frac{n_{i-1}}{n_i}=\frac{X_{i+1}-X_i}{X_i-X_{i-1}}\leqslant\frac{\kappa+1}{\kappa}, \quad \kappa>0. \tag{21}$$

The ratio of the grid point distances of two neighbouring intervals is limited by the given expression with $\kappa \approx 2{\cdot}0$. This spatial smoothing is performed by replacing n_i by the numerically diffused counterpart

$$\tilde{n}_i = n_i - \kappa(\kappa+1)(n_{i+1} - 2n_i + n_{i-1}), \quad \kappa > 0. \tag{22}$$

Substitution into (20) leads to

$$\frac{\tilde{n}_{i-1}}{M_{i-1}} = \frac{\tilde{n}_i}{M_i}, \quad i = 2, \ldots, NP-1. \tag{23}$$

These $NP-2$ equations are completed by prescribing equal lengths for the first and second and respectively the last two intervals:

$$n_0 = n_1, \qquad n_{NP-1} = n_{NP} \tag{24}$$

The last step is the temporal smoothing of the grid motion by replacing $\tilde{n}_i$ by $\hat{n}_i$:

$$\hat{n}_i = \tilde{n}_i + \tau_G \frac{\mathrm{d}\tilde{n}_i}{\mathrm{d}t}, \tag{25}$$

where τ_G is the time constant of the moving grid points. The algebraic system of the node positions (18), which was replaced in several steps by equations for the node concentrations (20) and (23), now results in

$$\frac{\hat{n}_{i-1}}{M_{i-1}} = \frac{\hat{n}_i}{M_i} \quad i = 2, \ldots, NP-1. \tag{26}$$

The effect of this formulation is that the grid adapts on the time scale τ_G and neglect disturbances on shorter time scales. The final step is to formulate (26) for the grid point positions $X_i(t)$. This system together with (24) and (25) leads to the implicit quasi-linear ordinary differential equation system for the moving nodes

$$\begin{aligned} \dot{X}_{i-1} - 2\dot{X}_i + \dot{X}_{i+1} &= 0, \quad i = 1, NP, \\ \dot{X}_i &= 0, \quad i = 0, NP+1, \\ \tau_G \sum_{k=-2}^{2} a_{i,k} \dot{X}_{i+k} &= f_i(X_{i-2}, \ldots, X_{i+2}, U_{i-1}, \ldots, U_{i+1}), \quad i = 2, \ldots, NP-1, \end{aligned} \tag{27}$$

with

$$\begin{aligned} a_{i,-2} &= a_{i,-2}(X_{i-2}, \ldots, X_i, U_{i-1}, U_i), \\ a_{i,-1} &= a_{i,-1}(X_{i-2}, \ldots, X_{i+1}, U_{i-1}, \ldots, U_i), \\ a_{i,0} &= a_{i,0}(X_{i-1}, \ldots, X_{i+1}, U_{i-1}, \ldots, U_i), \\ a_{i,2} &= a_{i,2}(X_{i-1}, \ldots, X_{i+2}, U_{i-1}, \ldots, U_i), \\ a_{i,2} &= a_{i,2}(X_i, \ldots, X_{i+2}, U_i, U_{i+1}), \quad i = 2, \ldots, NP-1, \\ f_i &= \frac{\tilde{n}_{i-1}(X_{i-2}, \ldots, X_{i+1})}{M_{i-1}(X_{i-1}, X_i, U_{i-1}, U_i)} - \frac{\tilde{n}_i(X_{i-1}, \ldots, X_{i+2})}{M_i(X_i, X_{i+1}, U_i, U_{i+1})}, \quad i = 2, \ldots, NP-1. \end{aligned}$$

The monitor function M_i is evaluated at the centre of the interval using the values of x and U at i and $i+1$. The formulation (27), which is used instead of (18), describes the movement of the grid

point at a location X_i by considering the node velocity of the neighbouring nodes X_{i+k}, $k=-2,-1$, 1 and 2. The combination of (17) and (27) gives rise to the semidiscretized formulation of (7) with a moving grid in the abstract notation

$$\mathbf{A}(\mathbf{Y})\dot{\mathbf{Y}}=\mathbf{F}(\mathbf{Y}), \tag{28}$$

with the $(2NP+4)\times(2NP+4)$ matrix $\mathbf{A}$ and the solution vector

$$\mathbf{Y}(t)=(U_0(t), X_0(t), \ldots, U_i(t), X_i(t), \ldots, U_{NP+1}(t), X_{NP+1}(t))^{\mathrm{T}}.$$

The time discretization is carried out with a solver for initial value problems of DAE systems.

4. COMPUTATIONAL RESULTS

The numerical method described above was applied to the non-stationary flame propagation problem (1)–(5). This results in the following differential–algebraic equation system of dimension $N=(NP+2)\times(NST+4)$:

$$\mathbf{B}(\mathbf{Y})\dot{\mathbf{Y}}=\mathbf{F}(\mathbf{Y}), \qquad \mathrm{Y}(0)=\mathbf{Y}_0, \tag{29}$$

where $\mathbf{B}$ is a singular $N\times N$ matrix with an upper and lower bandwidth of $2\times(NST+4)$, $\mathbf{F}$ is a vector of dimension $(NP+2)\times(NST+4)$ containing L_Δ from (17) and f_i from (27),

$$\mathbf{Y}=(Y_{1,0}, \ldots, Y_{NST,0}, \psi_0, p_0, T_0, z_0, \ldots, Y_{1,i}, \ldots, Y_{NST,i},$$
$$\psi_i, p_i, T_i, z_i, \ldots, Y_{1,NP+1}, \ldots, Y_{NST,NP+1}, \psi_{NP+1}, p_{NP+1}, T_{NP+1}, z_{NP+1})^{\mathrm{T}}$$

is the solution vector,

$$\begin{aligned} Y_{i,j}&=Y_i(\psi_j, t), \quad i=1, \ldots, NST,\\ p_j&=p_j(\psi_j, t),\\ T_j&=T(\psi_j, t),\\ z_j&=z(\psi_j, t),\\ \psi_j&=\psi_j(t), \qquad j=0, \ldots, NP+1. \end{aligned}$$

The spatial dicretization of equation (4) leads to an algebraic equation which causes a singular matrix $\mathbf{B}$. The implicit time discretization is performed with DASSL, a DAE solver using backward difference schemes with variable order and time step. The choice of an implicit time discretization is motivated by the large stiffness of (29) due to the presence of the reaction rate source terms $\dot{r}_i$ in (1) and (2) and the small grid point distances. The grid parameter τ_G is another quantity which introduces stiffness into (29), as described in Reference 15. The specific monitor function is defined by

$$m(\psi, t)=\left[1+c_t\left(\frac{\partial T}{\partial \psi}(\psi, t)\right)^2+c_y\sum_{i=1}^{NST}\left(\frac{\partial Y_i}{\partial \psi}(\psi, t)\right)^2\right]^{1/2}, \quad c_t, c_y\geqslant 0. \tag{30}$$

The parameters c_t and c_y are weight coefficients which are necessary to scale the problem.

The computational results presented in this section show two different situations of one-dimensional non-stationary laminar flame propagation and ignition in a closed vessel. In the first case these processes are simulated in a premixed H_2/air mixture where the flame propagates into the unburnt gas until it reaches the wall. In the other case the simulation is performed for a premixed O_3/O_2 mixture where the homogeneous ignition of the unburnt gas stops the flame

propagation before it reaches the wall. During the whole computation the parameter τ_G which controls the temporal smoothness of the grid motion was set to 10^{-9} s, while the spatial smoothing parameter was set to $\kappa = 2$. The velocity of the grid depends on the chosen value of τ_G. A large τ_G results in a grid moving too slowly which cannot follow the steep solution gradients. As a consequence, the time derivative of the solution values in the moving grid points is large and the DAE solver has to take smaller time steps. On the other hand, a value of τ_G that is too small generates spurious oscillations in the grid point trajectories. This is discussed in Reference 15 where the parameter λ used there is comparable to $1/\tau_G$. The parameter κ was selected in a problem-independent way based on suggestions made in References 11 and 13. Numerical experiments indicate that τ_G should be smaller than the time steps of the time discretization. Finally, the only parameters which have to be chosen by the user are the weight coefficients c_t and c_y and the fixed number of interior grid points, NP.

All computations were performed using the FORTRAN subroutine packages TRANFIT and CHEMKIN for the evaluation of λ, V_i, c_p, c_{p_i}, h_i and the chemical production rate $\dot{r}_i$ in terms of the state variables T, p and Y_i, $i = 1, \ldots, NST$, and their gradients.[16,17] These packages allow the flexible incorporation of detailed chemical kinetics and transport processes.

4.1. Ignition and flame propagation in a premixed H_2/air mixture

The simulation of ignition and flame propagation processes in an H_2/air mixture exhibits the presence of various solution gradients in different regions while moving in a one-dimensional way through a vessel 1·0 cm in length. The reaction mechanism involves 26 elementary reactions of nine chemical species.[18] The initial uniform species mass fractions are $Y_{O_2} = 0{\cdot}2253$, $Y_{H_2} = 0{\cdot}028678$ and $Y_{N_2} = 0{\cdot}746022$, while the other initial mass fractions were set to zero. The initial temperature and pressure were set to $T_0 = 700$ K and $p_0 = 1$ bar. The mixture was ignited with a sufficient energy supply located in a region of 0·02 cm width at the boundary $z_0 = 0$ for a period of $t_i = 5{\cdot}0$ μs. The density of the energy source was set to $D = 5 \times 10^6$ erg cm^{-1}. After

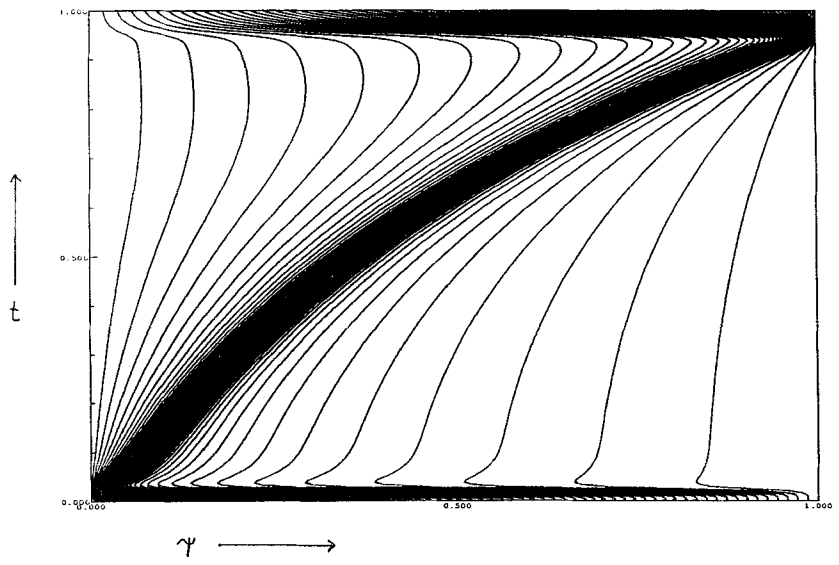

Figure 1. Grid point trajectories in Lagrangian co-ordinates for an H_2/air mixture with initial temperature $T_0 = 700$ K and pressure $p_0 = 1$ bar

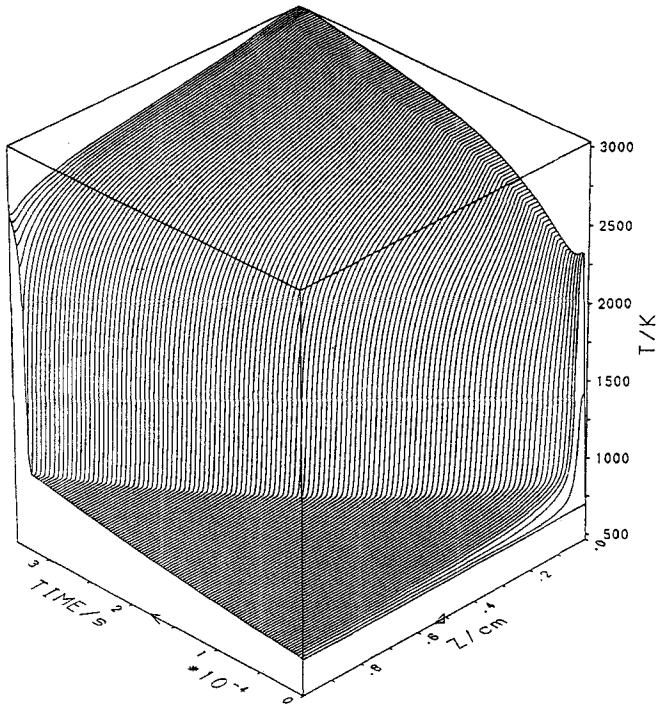

Figure 2. Time evolution of the temperature for an H_2/air mixture with initial temperature $T_0 = 700$ K and pressure $p_0 = 1$ bar

a short induction period the ignition of the mixture occurs in this small region and a flame propagation starts. The evolution of the whole process is demonstrated in Figures 1–3. The grid motion in the Lagrangian co-ordinate system is shown in Figure 1. The computation is performed on a uniform grid consisting of 70 grid points. The coefficients c_t and c_y for the monitor function (30) were set to $c_t = (\psi_{max}/3000\ \text{K})^2$ and $c_y = (\psi_{max})^2$. The grid adaption starts locally in the vicinity of the heated region. This process is accelerated and extended by the rapid formation of a large temperature gradient during the ignition period (Figure 2), which forces the grid points to move into that region. At the moment of ignition nearly 45 grid points are concentrated in a small region 1/25th of the vessel length. During the following flame propagation the high spatial resolution of the flame and the reaction zone is maintained. This is demonstrated in Figure 3, which shows the concentration of the intermediate species HO_2. It has a very sharp peak profile which is associated with the flame front. This moving structure is sufficiently resolved during the entire flame propagation, which continues until the flame reaches the wall after 150 μs. The curvature of the grid trajectories in Lagrangian co-ordinates implies an increasing mass flux due to the relation

$$\frac{\partial \psi}{\partial t} = -\rho v.$$

This behaviour can be explained by the accelerated pre-reactions in the unburnt gas due to the temperature and pressure increases which are generated by the adiabatic expansion of the hot burnt gas. The typical computation time is 40 min on a SUN4 workstation and 4 min on a CRAY-YMP.

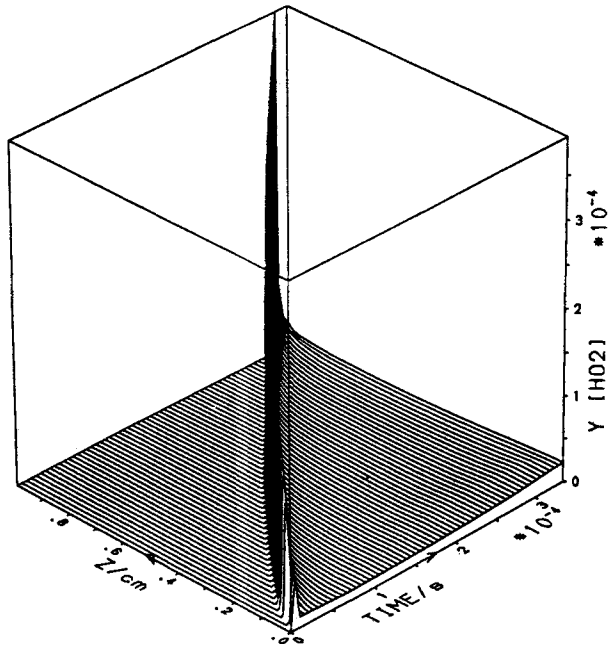

Figure 3. Time evolution of the HO_2 mass fraction for an H_2/air mixture with initial temperature $T_0 = 700$ K and pressure $p_0 = 1$ bar

4.2. *Ignition and flame propagation in a premixed O_3/O_2 mixture*

This simulation was performed in order to demonstrate the interdependence of laminar flame propagation and self-ignition in a closed vessel. The computation was performed with an initially uniform grid of 60 grid points. The weight coefficients for the monitor function were set to $c_t = (\psi_{max}/3000\ \text{K})^2$ and $c_y = 0$. The one-dimensional vessel has a length of 1 cm and the initial mass fractions are $Y_{O_3} = 0{\cdot}4$, $Y_{O_2} = 0{\cdot}6$ and $Y_O = 0$. The initial temperature $T_0 = 550\ K$ lies above the self-ignition temperature and the pressure is set to $p_0 = 1$ bar. A region of 0·04 cm length at the right boundary was supplied with energy until $t_i = 5\ \mu s$. The density of the energy source was set to $D = 5 \times 10^6\ \text{erg cm}^{-1}$. The kinetics of the system was described by a system of seven elementary reactions including three species.[18] The evolution of the system is presented in Figures 4–6. The ignition period is terminated after 3 μs and the propagation of the flame front starts after that time. The grid point trajectories in Figure 4 show the capability of the grid to follow the combustion wave. Nearly 30 grid points are concentrated in this region of high spatial activity which has a width of 3·6% of the total vessel length. The sufficient resolution of the temperature profile can be seen in Figure 5. During the period of flame propagation the DAE solver selects time steps of about 10^{-5} s. The typical flame propagation time based on the smallest grid spacing is 7×10^{-7} s. This indicates that the time step of the integration is limited neither by the characteristic unsteadiness time nor by the grid adaption time τ_G. The grid point trajectories in Figure 4 show an accelerated flame front before the flame propagation is terminated by the homogeneous ignition of the unburnt gas. The reason is that the expansion of the hot burnt gas in the closed vessel causes an adiabatic compression of the unburnt gas which results in temperature and pressure increases. The temperature and O_2 profiles in Figures 5 and 6 show the fast-vanishing gradients due to the rapid pre-reactions in front of the flame. Shortly after the

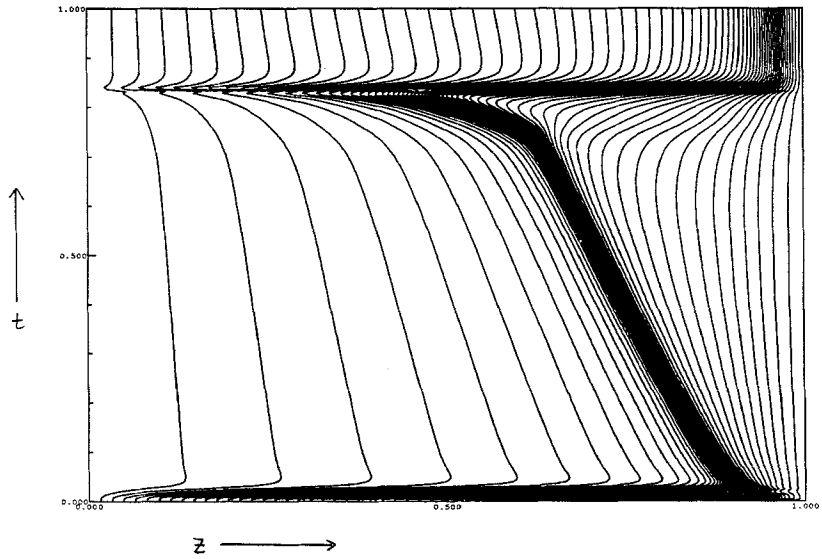

Figure 4. Grid point trajectories in Eulerian co-ordinates for an O_3/O_2 mixture with initial temperature $T_0 = 550$ K and pressure $p_0 = 1$ bar

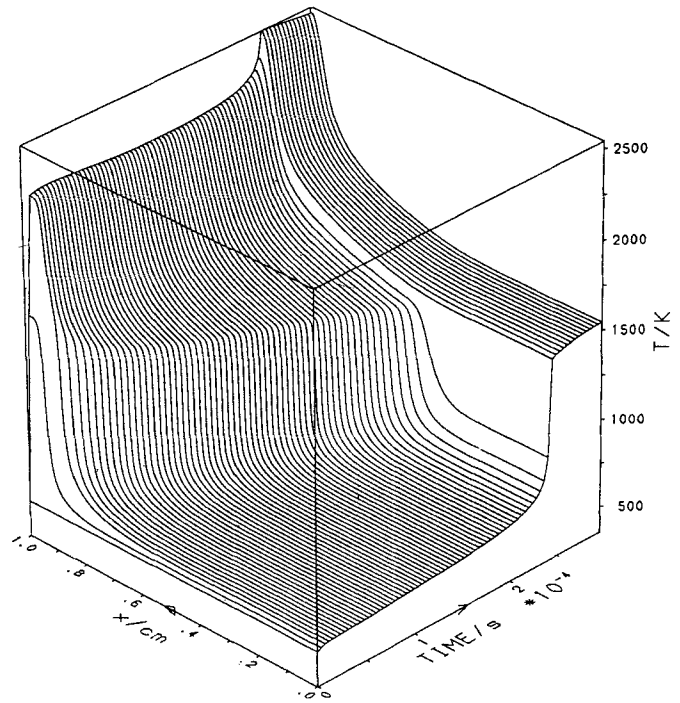

Figure 5. Time evolution of the temperature for an O_3/O_2 mixture with initial temperature $T_0 = 550$ K and pressure $p_0 = 1$ bar

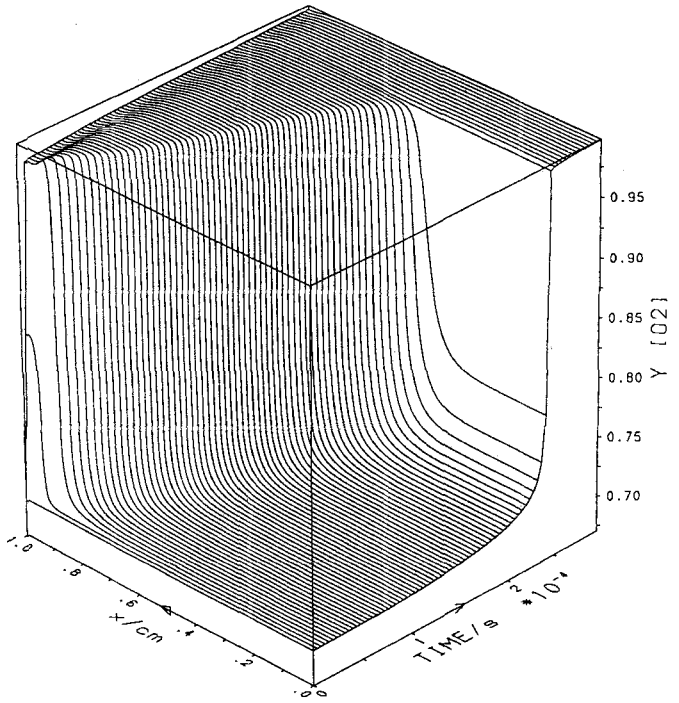

Figure 6. Time evolution of the O_2 mass fraction for an O_3/O_2 mixture with initial temperature $T_0 = 550$ K and pressure $p_0 = 1$ bar

homogeneous ignition the grid points are distributed according to the remaining temperature gradient which was created by the external heat supply. This gradient is smoothed out by heat conduction later on. The computation time for this simulation is 10 min on a SUN4 workstation and 1 min on a CRAY-YMP.

5. CONCLUSIONS

In this paper a detailed presentation of a fully implicit moving grid method and its application to two confined laminar one-dimensional flame propagation problems are given. The main emphasis is on a strong coupling between the solution of the approximated governing equations and the differential equations for a fixed number of grid points. The semidiscretization of these equations leads to a differential–algebraic system for the grid point position and the solution values in these nodes. This approach is motivated by the availability of solvers for the numerical solution of stiff differential–algebraic equations. In these solvers the time discretization is performed with implicit schemes. The computational efficiency is demonstrated by the large time steps taken by the solver during the propagation process and the high resolution of the various moving fronts. Although the formation of peaks and steep gradient regions was resolved, a drawback is that the rapid grid adaption requires small time steps during the formation process. Current investigations indicate that this moving grid method is also applicable to one-dimensional reacting shock waves and multiple-front propagation.

ACKNOWLEDGEMENTS

The authors gratefully acknowledge the financial support of the Deutsche Forschungsgemeinschaft and the opportunity to perform the calculations on the CRAY-YMP of the HLRZ, Jülich.

REFERENCES

1. E. S. Oran and J. P. Boris, 'Detailed modelling of combustion systems', *Prog. Energy Combust. Sci.*, **7**, 1–72 (1981).
2. R. J. Kee, L. R. Petzold, M. D. Smooke and J. F. Grcar, 'Implicit methods in combustion and chemical kinetics modelling', in J. U. Brackbill and B. I. Cohen (eds), *Multiple Time Scales*, Academic, New York, 1985, pp. 113–144.
3. R. D. Russel and J. Christiansen, 'Adaptive mesh selection strategies for solving boundary value problems', *SIAM J. Numer. Anal.*, **15**, 59–80 (1978).
4. V. Pereyra and E. G. Sewell, 'Mesh selection for discrete solution of boundary problems in ordinary differential equations', *Numer. Math.*, **23**, 261–268 (1975).
5. P. Deuflhard and U. Nowak, 'Extrapolation integrators for quasilinear implicit ODEs', *University of Heidelberg, SFB 123: Tech. Rep. 332*, 1985.
6. L. R. Petzold, 'A description of DASSL: a differential/algebraic system solver', in R. S. Stepleman (ed.), *Scientific Computing*, North-Holland, Amsterdam, 1983, pp. 65–68.
7. M. J. Baines and A. J. Wathen, 'Moving finite element methods for evolutionary problems. I. Theory', *J. Comput. Phys.*, **79**, 245–269 (1988).
8. I. W. Johnson, A. J. Wathen and M. J. Baines, 'Moving finite element methods for evolutionary problems. II. Applications', *J. Comput. Phys.*, **79**, 270–297 (1988).
9. A. J. Wathen and M. J. Baines, 'On the structure of the moving finite element equations', *IMA J. Numer. Anal.*, **5**, 161–182 (1985).
10. A. J. Wathen, 'Mesh-independent spectra in the moving finite element equations', *SIAM J. Numer. Anal.*, **23**, 797–814 (1986).
11. R. M. Furzeland, J. G. Verwer and P. A. Zegeling, 'A numerical study of three moving grid methods for one-dimensional partial differential equations which are based on the method of lines', *Report NM-R8806*, Centre for Mathematics and Computer Science, Amsterdam, 1988.
12. U. Maas and J. Warnatz, 'Ignition processes in hydrogen–oxygen mixtures', *Combust. Flame*, **74**, 53–69 (1988).
13. E. A. Dorfi and L. O'C. Drury, 'Simple adaptive grids for 1-D initial value problems', *J. Comput. Phys.*, **69**, 175–195 (1987).
14. J. Smoller, *Shock Waves and Reaction–Diffusion Equations*, Springer, New York, 1983.
15. J. M. Coyle, J. E. Flaherty and R. Ludwig, 'On the stability of mesh equidistribution strategies for time-dependent partial differential equations', *J. Comput. Phys.*, **62**, 26–39 (1986).
16. R. J. Kee, J. A. Miller and T. H. Jefferson, 'CHEMKIN: a general-purpose, problem-independent, transportable, Fortran chemical kinetics code package', *SANDIA National Laboratories Report SAND80-8003*, 1988.
17. R. J. Kee, J. Warnatz and J. A. Miller, 'A FORTRAN computer code package for the evaluation of gas-phase viscosities, conductivities, and diffusion coefficients', *SANDIA National Laboratories Report SAND83-8209*, 1983.
18. D. Kaufmann, *Ph.D. Dissertation*, University of Duisburg, 1989.